Acta Materialia 199 (2020) 523–529

Contents lists available at ScienceDirect

Acta Materialia

journal homepage: www.elsevier.com/locate/actamat

Full length article

Triplet grain growth in *a*-texture polycrystalline ZnO thin films

A. Brian Aebersold[a], Cécile Hébert[a,b], Duncan T.L. Alexander[a,b,*]

[a] Interdisciplinary Centre for Electron Microscopy (CIME), École Polytechnique Fédérale de Lausanne (EPFL), Lausanne, Switzerland
[b] Electron Spectrometry and Microscopy Laboratory (LSME), Institute of Physics (IPHYS), École Polytechnique Fédérale de Lausanne (EPFL), Lausanne, Switzerland

ARTICLE INFO

Article history:
Received 28 March 2020
Revised 19 August 2020
Accepted 24 August 2020
Available online 28 August 2020

Keywords:
Polycrystalline thin films
ZnO
Grain triplet
Renucleation
Twinning

ABSTRACT

A growth of grain triplets is identified in vapor deposited, *a*-texture polycrystalline zinc oxide thin films, using a combination of transmission electron microscopy-based automated crystal orientation mapping and high-resolution imaging. Each triplet consists of three wurtzite phase grains, coordinated to near tetrahedral relative growth angles by the close-packed planes of a few nanometer diameter core of metastable zinc blende phase ZnO located at their triple junction. The triplets are aligned such that two of the grains have their fast growing [2 $\bar{1}$ $\bar{1}$ 0] axes (near-) parallel to the substrate normal, and so coarsen under the principle of competitive grain growth. In contrast, growth of the third grain with a (1 0 $\bar{1}$ 3) texture is impeded, such that it forms a small wedge between the ends of its two larger neighbors. Remarkably, all three boundaries between the grains adhere to a [2 $\bar{1}$ $\bar{1}$ 0]/(0 1 $\bar{1}$ 3) coherent twin orientation relationship, which corresponds to a grain geometry that is incommensurate with a perfect crystallographic nature. This coherency is primarily achieved via the small grain having an orientation that rotates internally by 10±2° across its volume, when going between the two interfaces formed with the neighboring large grains. The energy associated with this structural distortion is compensated by the formation of the coherent twin boundaries, such that the triplets are a stable or semi-stable growth form that are abundant in the film. The small (1 0 $\bar{1}$ 3) texture grains may renucleate persistently, taking either of two possible orientations from the underlying tetrahedral coordination. By developing a phenomenological model for the triplet geometry and form, we associate these two orientations to small hexagonal caps and angled wedges seen in the surface morphology of the film. These findings potentially carry relevance for a wide range of vapor deposited compact films and free-standing nanostructures of wurtzite phase octet binary semiconductor compounds. We therefore believe that these insights can stimulate new research, for instance to obtain a more fundamental understanding of the growth mechanisms at the atomistic level.

1. Introduction

In any formation of crystalline matter, the nucleation and growth of the new crystal involves a balance of the free energy of formation of its volume versus an energetic penalty for the creation of its interfaces [1]. One consequence of this is that the nature of the interfaces that are created, and their associated energies, can drive the formation of crystal grains with specific morphologies and crystallographic orientation relationships. This phenomenon applies across fields from physical metallurgy to the growth of semiconductor nanowires [2–6], or formation of vapor-deposited thin films of the type studied here [7]. A classical example is from solid state precipitation, when growing crystals preferentially adopt forms that maximize low energy coherent interfaces, where there is a matching of the atomic structures of the two neighboring crystal grains along their boundary, while growing fast along a higher energy and more atomically mobile incoherent boundary. This partially coherent combination leads to anisotropic growth, as seen in cases such as the formation of Widmanstätten-type kamacite precipitates in iron-rich meteorites and ferrite precipitates in steel alloys, or the growth of plate-shaped θ' precipitates in Al-Cu alloys [2,3]. In this article, we report a strong influence of coherent boundaries on the nanometric formation and growth of ZnO grains, however in the very

* Corresponding author at: EPFL SB IPHYS LSME, PH D2 344, Station 3, CH-1015 Lausanne, Switzerland.
E-mail addresses: duncan.alexander@epfl.ch, dtla@cantab.net (D.T.L. Alexander).

https://doi.org/10.1016/j.actamat.2020.08.068

different system of low-pressure metal–organic chemical vapor deposition (LP-MOCVD) of an *a*-texture polycrystalline ZnO thin film.[1] The boundaries correspond to low-energy coherent twins, and are created during the growth of wurtzite grains that are coordinated into a triplet formation by zinc blende cores with a few nm in diameter. While zinc blende structured ZnO is itself is metastable [12,13], this triplet grain structure grows in a stable or semi-stable manner. This work builds upon two observations that we have previously reported for LP-MOCVD grown polycrystalline ZnO thin films: firstly, the role of a similar wurtzite–zinc blende polytypism in the growth of *c*-texture films [14]; secondly, stable growth of *a*-texture twinned grains, and persistent renucleation of grains with a minor $(1\ 0\ \bar{1}\ 3)$ texture, during growth of various *a*-textured films [15,16]. We finally develop a phenomenological model of the triplet morphology and growth orientation which explains aspects of the surface morphology of these films that were not previously understood.

2. Experimental methods

The study focuses on a polycrystalline ZnO thin film that was grown on a glass substrate by LP-MOCVD using precursor gasses of diethylzinc and H_2O in a 1:1 ratio, at a pressure of 0.35 mbar, total gas flow of 150 sccm and a substrate temperature of 170 °C (see [17] for details of the deposition chamber). The film is analyzed using various electron microscopy methodologies. Scanning electron microscopy (SEM) is applied to image the surface morphology of the as-deposited film, using a Zeiss Merlin microscope operated at 8 kV. Transmission electron microscopy (TEM)-based automated crystal orientation mapping (ACOM) is used to study the nanometric size, shape and orientation of different grains in the film. The ACOM is performed with a NanoMEGAS ASTAR system [18] installed on a JEOL JEM 2200FS microscope operated at 200 kV, and is applied to both cross-section [19] and "double-wedge" plan-view [20] TEM samples.

While comprehensive details on the ACOM acquisition and data processing are presented in our previous research [15,16], we briefly reiterate the main acquisition and data processing parameters. The spot diffraction patterns for ACOM were produced by a quasi-parallel (0.8 mrad convergence angle) beam with 2 nm diameter, which was created by using JEOL's nano-beam diffraction mode. The maps were recorded using a square grid with 2 nm step size for plan view maps and 5 nm for cross-section maps. The patterns were recorded at a speed of 100 patterns per second using ASTAR's dedicated Stingray camera. Diffraction pattern indexing was done with ASTAR's indexing procedure. Further post-processing included a median filter as described by Kobler et al. [21]. The orientation maps and pole figures shown here were all made using MTEX [22]. MTEX was further used for automated identification of boundaries close to a twin boundary orientation relationship. Prior to this, grains were reconstructed in MTEX with a misorientation threshold of 3°. Afterwards, grains with less than 20 pixels (i.e. $<$ 10 nm in equivalent circle grain diameter) or grains with less than 25% of their pixels having a reliability index above 15 were removed in order to improve data validity. The reliability index is calculated by the ASTAR indexing. It provides a measure of the uniqueness of the selected orientation match. Values less than 15 are typically an indication that there could be an issue with the uniqueness of the identified orientation [21,23]. Such low reliabilities are usually encountered when there is an overlap of different grains within the electron beam path, which typically occurs at grain boundaries.

[1] These films are developed as transparent conductive oxide electrodes for optoelectronic applications, as for instance related in [8–11].

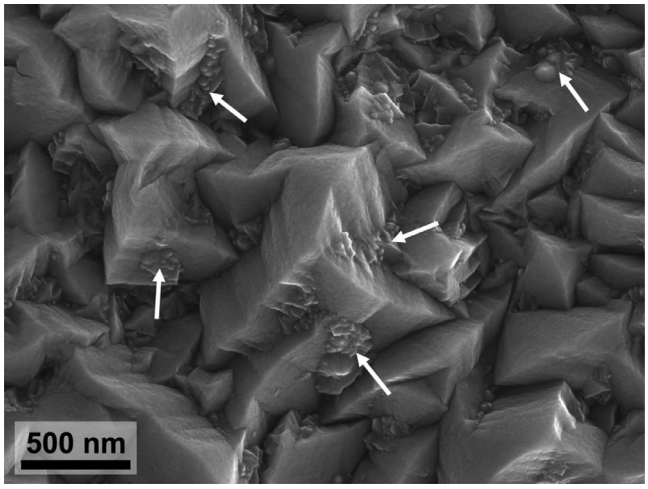

Fig. 1. Surface morphology of the LP-MOCVD grown polycrystalline ZnO thin film. The arrows indicate some of the small features, mostly existing in the interstices of the large pyramidal grains, that are incommensurate with the formation of the film according to a classical model of competitive grain growth. The image was recorded using SEM with the in-lens secondary electron detector.

All presented inverse pole figure orientation maps, where the orientation is encoded by color, have been multiplied with a gray scale reliability index map. This is useful for a better visualization of grain boundaries. The gray scale has been chosen such that all points with reliabilities larger than 15 appear white and points between 0 and 15 go linearly from black to white. The precision of spot pattern orientation mapping has been shown to be ±1° for absolute orientations and ±1.4° for misorientations [24]. We therefore specify our misorientation measurements with a conservative error of ±2°.

Correlative high-resolution (HR-)TEM studies are performed on a FEI Tecnai Osiris microscope operated at 200 kV.

3. Results and discussion

Fig. 1 presents a secondary electron SEM image of the surface of the ZnO film, which was grown to a thickness of ~ 2.5 μm. The morphology is dominated by large pyramidal structures. These correspond to twinned grains that have grown with orientations close to the primary $(2\ \bar{1}\ \bar{1}\ 0)$ texture of the film (i.e. a $[2\ \bar{1}\ \bar{1}\ 0]$ fiber texture parallel to the substrate normal direction), and are the grains that have been "successful" in the process of competitive grain overgrowth via which the film microstructure has evolved [16]. According to this model, as first proposed by van der Drift [25], the surface morphology of the mature film should consist only of such structures, since otherwise oriented grains with differing surface structures will have been eliminated during the competitive process. Nevertheless, as can be seen in Fig. 1, careful analysis of the surface identifies other features, typically existing in the valleys or interstices between the large pyramids: small conical caps and narrow angled wedges. Based on the analysis and segmentation of ACOM data acquired on the same film, in Section 3.4 we develop a phenomenological model via which these extra features can be explained. We note that all of the features shown in Fig. 1 are characteristic of the general morphology across the deposited film surface. In order to demonstrate the uniformity of the film surface morphology, further SEM images are presented in the supplementary Figs S 1 and S 2.

3.1. Identification of triplets in ACOM data

As the basis for this study, Fig. 2 presents inverse pole figure orientation maps of plan view slices at heights of 60 nm (a) and

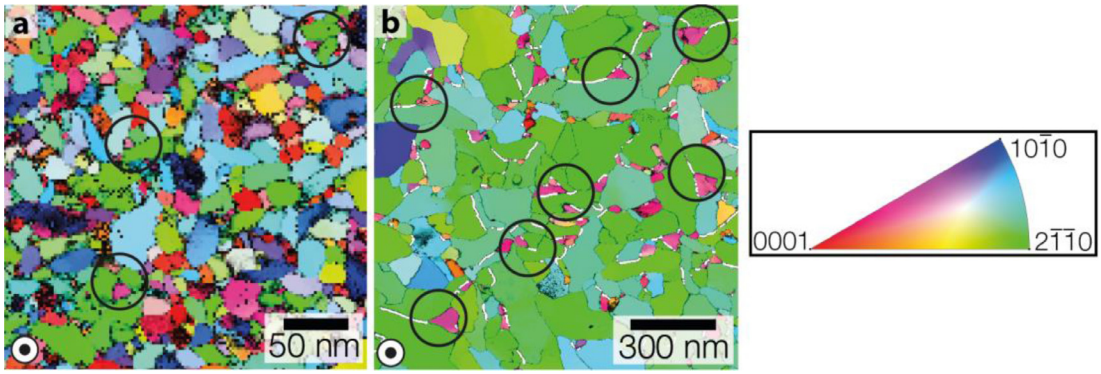

Fig. 2. Plan-view orientation maps at two film heights. The ZnO thin film was recorded in plan-view geometry using a double-wedge sample from film heights of (a) 60 nm and (b) 850 nm. The orientation maps are colored with respect to the film growth direction (i.e. substrate normal) according to the color map on the right. Grain boundaries corresponding to a (0 1 $\bar{1}$ 3) twin boundary orientation relationship (within a tolerance of 3°) have been marked in white. Various grain triplets, each consisting of a pink-rose colored (1 0 $\bar{1}$ 3) oriented renucleating grain wedged between a green-colored *a*-textured twin pair, are indicated using black circles. (For interpretation of the references to color in this figure legend, the reader is referred to the web version of this article.)

850 nm (b) within the film, recorded using ACOM from a double-wedge TEM sample. In the 850 nm height map, the largest grains are primarily colored green, corresponding to the (2 $\bar{1}$ $\bar{1}$ 0) major texture of the film, with small, rose-pink colored grains that correspond to the minor (1 0 $\bar{1}$ 3) texture component. Following the procedure presented in [15,16], white boundaries are used to mark pairs of grains that conform to a [2 $\bar{1}$ $\bar{1}$ 0]/(0 1 $\bar{1}$ 3) coherent twin orientation relationship (which henceforth are simply denoted as "(0 1 $\bar{1}$ 3) twins"). As well as this segmentation showing that there is an abundance of coherent twin pairs, careful inspection of the data reveals that there is a further correlation, in that there is a strong coincidence of the rose-pink (1 0 $\bar{1}$ 3) textured grains with the green *a*-textured twinned pairs. Specifically, each of the (1 0 $\bar{1}$ 3) textured grains is typically a triangle wedged in a gap between the ends of a twinned pair, with its apex sprouting from the twin boundary. Together, these three grains form a triplet. The triplet correspondence is not unique to this height in the film. Various examples showing this relationship are circled in black on Fig. 2, indeed showing that such triplets already exist in part (a), the map recorded at a 60 nm film height.

As described in more detail in Section 3.3, orientation analysis finds that, within each triplet, the three grains have angles between them that fall within a certain range. For the large, twinned grains, this is 64±2°, corresponding closely to the (0 1 $\bar{1}$ 3) twin relationship [26–28]. Each small grain in turn maintains an angle of 72±2° with either of the (2 $\bar{1}$ $\bar{1}$ 0) oriented grains between which it is wedged. The misorientations of 12 such triplets have been measured, as shown in Table S 1 of the supplementary data, giving values that confirm the generality of this angular relationship. Taken together, the three angles are close to having a tetrahedral correspondence, covering three out of four possible directions and being near the ideal tetrahedral angle of 70.5°. HR-TEM imaging at the triple junction of the triplet gives a clear indication as to why, as explained in the next section.

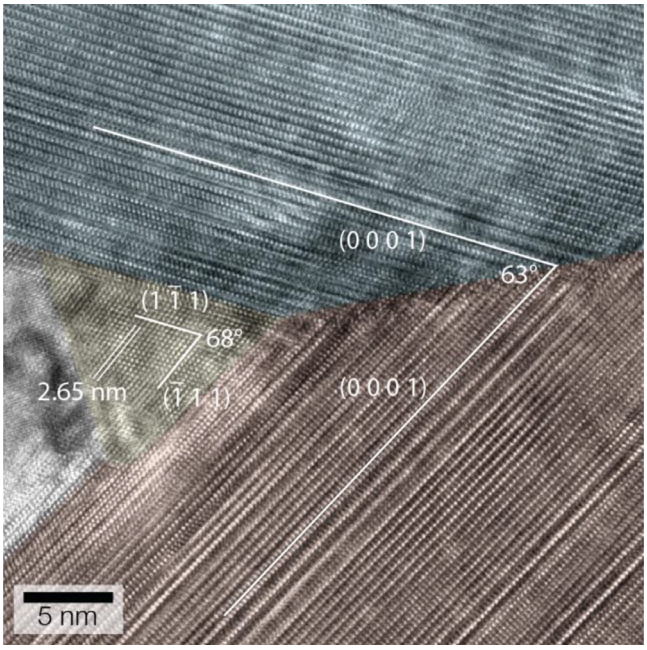

Fig. 3. HR-TEM image from the triple junction of a representative grain triplet. Color is superimposed to help distinguish the different grains. The sample has been aligned on the shared [2 $\bar{1}$ $\bar{1}$ 0] zone axis of the *a*-textured twin pair, the grains of which are colored in blue and brown. At the junction of these two grains with the "renucleated" (1 0 $\bar{1}$ 3) oriented grain (in gray), a small, triangular core of [1 1 0] oriented zinc blende phase ZnO is observed, as colored in yellow. The orientations and angles between various end-on planes in the three grains are indicated. (For interpretation of the references to color in this figure legend, the reader is referred to the web version of this article.)

3.2. HR-TEM analysis of triple junction

Fig. 3 shows a representative HR-TEM image of a grain triplet triple junction. The twinned pair of *a*-texture grains have been aligned on their common [2 $\bar{1}$ $\bar{1}$ 0] zone axis. At the center of the triple junction, a few nanometer diameter core of zinc blende phase ZnO is seen along the [1 1 0] zone axis. It is oriented in such a way that it will coordinate the growth of each of the surrounding wurtzite grains on its tetrahedrally-related {1 1 1} close packed planes. It is noted that such zinc blende cores were systematically found when performing HR-TEM imaging on a number of triple points. We have already observed a similar polytypism mechanism, in which a zinc blende core leads to the growth of tetrahedrally-related wurtzite grains, during growth of *c*-textured LP-MOCVD ZnO thin films, when the basal plane of each wurtzite grain originates from the close-packed planes of the zinc blende core [14]. Nevertheless, there are some distinct differences in the two cases. In the *c*-textured film, the original *c*-textured grain and the new grains, (which in turn grow at an angle to the fast growth axis), maintain more perfect tetrahedral angles. Further, in this *a*-texture case, the two principal twinned grains are oriented on the fast growth axis and hence are "successful" grains, and which form the primary pyramidal growth structures on the surface (Fig. 1).

As found with the ACOM, the HR-TEM image of Fig. 3 confirms that the two large grains are rotated away from a perfect tetrahedral angle to achieve a 63±1° angle between their (0 0 0 1) basal planes, corresponding to a perfect coherent twin relationship. This points to a significant energetic stabilization by the formation of a coherent boundary, even if the rotation implies that there must be significant stress/strain in the zone immediately around the zinc blende core. Indeed, the local stress is such that the angle between the {1 1 1} zinc blende planes that nucleate these two grains is compressed from the ideal 70.5° to a measured 68±1°. We note that this observation is the first experimental evidence of a direct link between zinc blende-wurtzite polytypism and the formation of (0 1 $\bar{1}$ 3) twin boundaries in ZnO, as was proposed by Ding et al. to explain the formation of free-standing ZnO nanowires made of twinned wurtzite grains [26,29]. Further, considering that grain triplets are observed even at the low film height of 60 nm, see Fig. 2(a), it appears that the zinc blende already forms during or just after initial nucleation on the substrate, tetrahedrally coordinating wurtzite grains such that a few tens of nanometers above the nucleation region a large fraction of (0 1 $\bar{1}$ 3) twin grain pairs/grain triplets are already created. The (0 1 $\bar{1}$ 3) twin formation derives from the interface having the lowest energy boundary configuration for wurtzite structures, as was predicted using atomistic simulations of GaN [28]. This strong energetic stabilization by twinning produces another aspect in the triplet formation which is distinctly more surprising, as we identify via analysis of ACOM data in the next section.

3.3. ACOM analysis of triplet interface geometry

The pole figures in Fig. 4 show the orientation configuration of a representative grain triplet, as measured using ACOM in a plan-view sample geometry. Part (b), the {2 $\bar{1}$ $\bar{1}$ 0} pole figure, indicates that each possible pair from the three grains are close to sharing common ⟨2 $\bar{1}$ $\bar{1}$ 0⟩-type axes. At the triple junction, the two large *a*-texture grains are related by a 63±2° misorientation (conforming to the coherent twinning), and the small grain forms an angle of 71±2° & 73±2° with the two large grains respectively. The twinning of the two large grains is confirmed by the {0 1 $\bar{1}$ 3} pole figure of Fig. 4(c), with them sharing a twinning plane parallel to the boundary of the two grains, while the small grain is some degrees off from sharing a {0 1 $\bar{1}$ 3}-type plane with either of the larger neighboring grains. However, remarkably, the small grain itself does not have a constant orientation across its volume. As seen in Fig. 4(d), it is strongly distorted, with an orientation that rotates by several degrees from one side to the other. We study this grain rotation by plotting the {2 $\bar{1}$ $\bar{1}$ 0} and {0 1 $\bar{1}$ 3} pole figures along a chord across the grain, further away from the triple junction, see Fig. 4(e)–(h). The grain rotation along the chord measures as large as about 10° within a distance of 75 nm. Further, by obtaining shared {0 1 $\bar{1}$ 3} twin planes and ⟨2 $\bar{1}$ $\bar{1}$ 0⟩ axes with the neighbor at each end of the chord, the rotation is such that the local orientation of the small grain achieves a {0 1 $\bar{1}$ 3} twin orientation relationship with both of its neighboring grains. Therefore, we conclude that this rotational distortion is driven by the formation of {0 1 $\bar{1}$ 3} coherent twin boundaries between the small grain and the large grains between which it is wedged, whose low energy compensates for the small grain's structural distortion, as its size and hence grain boundary area increases. Equally, due to its triangular shape, as it grows away from the triple junction, the distance between its two possible twin interfaces increases, giving a counterbalancing effect in that the net rotational strain needed to form the twin boundaries reduces. Unfortunately, the high index zone axis of the small grains in the double wedge TEM sample precludes a higher resolution analysis of the mechanism by which the grain rotation is achieved, for instance whether it is via pure rotational lattice strain or via dislocations arranged to produce consecutive low angle grain boundaries through the grain's volume.

3.4. Triplet growth discussion and model

By appropriating a nature in which all three grains are interfaced by low energy coherent boundaries, the ZnO triplets are a growth configuration that is favorable under the film's growth conditions, as judged by their abundance, e.g. see Fig. 2(b). While this growth favors the formation of low energy boundaries, the exposed tops of the *a*-textured grains present fine surface terraces (hypothesized to result from dense arrays of internal stacking faults), which should provide easy adatom absorption, resulting in high *a*-axis growth mobility and the observed growth anisotropy [17]. A somewhat similar triplet configuration was previously identified in Co–Ni electrodeposited films using three-dimensional electron backscatter diffraction analysis [30]. However, in that case, the hexagonal close packed grains in the triplet formed one coherent twin boundary, one incoherent twin boundary, and one large-angle grain boundary; a less surprising scenario than the internal grain rotation to achieve three coherent twin boundaries for the ZnO case described here.

As the film grows thicker, it is expected that the (1 0 $\bar{1}$ 3) oriented grains in each triplet remain small in lateral size compared to the (2 $\bar{1}$ $\bar{1}$ 0) oriented twins, because their fast growth axes are angled far away from the substrate normal, and so their growth will be impeded or blocked in the competitive grain overgrowth process [16,25]. Once one grain is blocked and its growth stops, the zinc blende core provides a site to nucleate a new grain, leading to the repetitive renucleation of the (1 0 $\bar{1}$ 3) textured grains. Their persistence means that the triplets effectively grow in a stable or semi-stable manner, as now demonstrated with analysis of ACOM data recorded from a cross-section TEM sample. In Fig. 5(a), showing an orientation map across the whole film thickness, an ellipse indicates the stable case, where a narrow grain of (1 0 $\bar{1}$ 3) texture has grown vertically and elongated between two columnar (2 $\bar{1}$ $\bar{1}$ 0) textured grains, which themselves were verified to be in a (0 1 $\bar{1}$ 3) twin orientation relationship with each other. This case may actually be more common than its singular observation suggests, since the likelihood of precisely sectioning such a narrow grain along its major axis is rather small. In comparison, just above this, the black circle marks the semi-stable case, in which the (1 0 $\bar{1}$ 3) textured grains do not grow very long, but instead repeatedly re-nucleate between twinned *a*-texture grains.[2]

Fig. 5(b) shows this region of re-nucleating grains at a higher magnification. It is pointed out that the low reliability on the left-hand region is due to an unfavorable orientation of the grain; nonetheless the orientation found is considered to be correct, since within the same grain there are high-reliability points in the vicinity where the grain orientation is only slightly different. Accompanying this, Fig. 5(c) shows the orientations of the different grains, and the *a*-texture twinned pair, on a {2 $\bar{1}$ $\bar{1}$ 0} pole figure. Analysis of this pole figure finds that each (1 0 $\bar{1}$ 3) textured grain adopts one of two possible orientation variants. This can be understood straightforwardly from their growth via the tetrahedral coordination by the zinc blende core. Two facets of the tetrahedron are connected to the (2 $\bar{1}$ $\bar{1}$ 0) textured grains, leaving two other facets on which new (1 0 $\bar{1}$ 3) textured grains may renucleate, thereby resulting in two possible orientations for these grains.

As a final step, we implicate these two possible orientations of the renucleating (1 0 $\bar{1}$ 3) grains in a phenomenological model

[2] We note that only the semi-stable formation of the (0 1 $\bar{1}$ 3) textured grains corresponds fully with our previous denotation of them as forming by renucleation [15,16]. That both stable and semi-stable growth is observed demonstrates the relative complexity of the microstructure formation in this system.

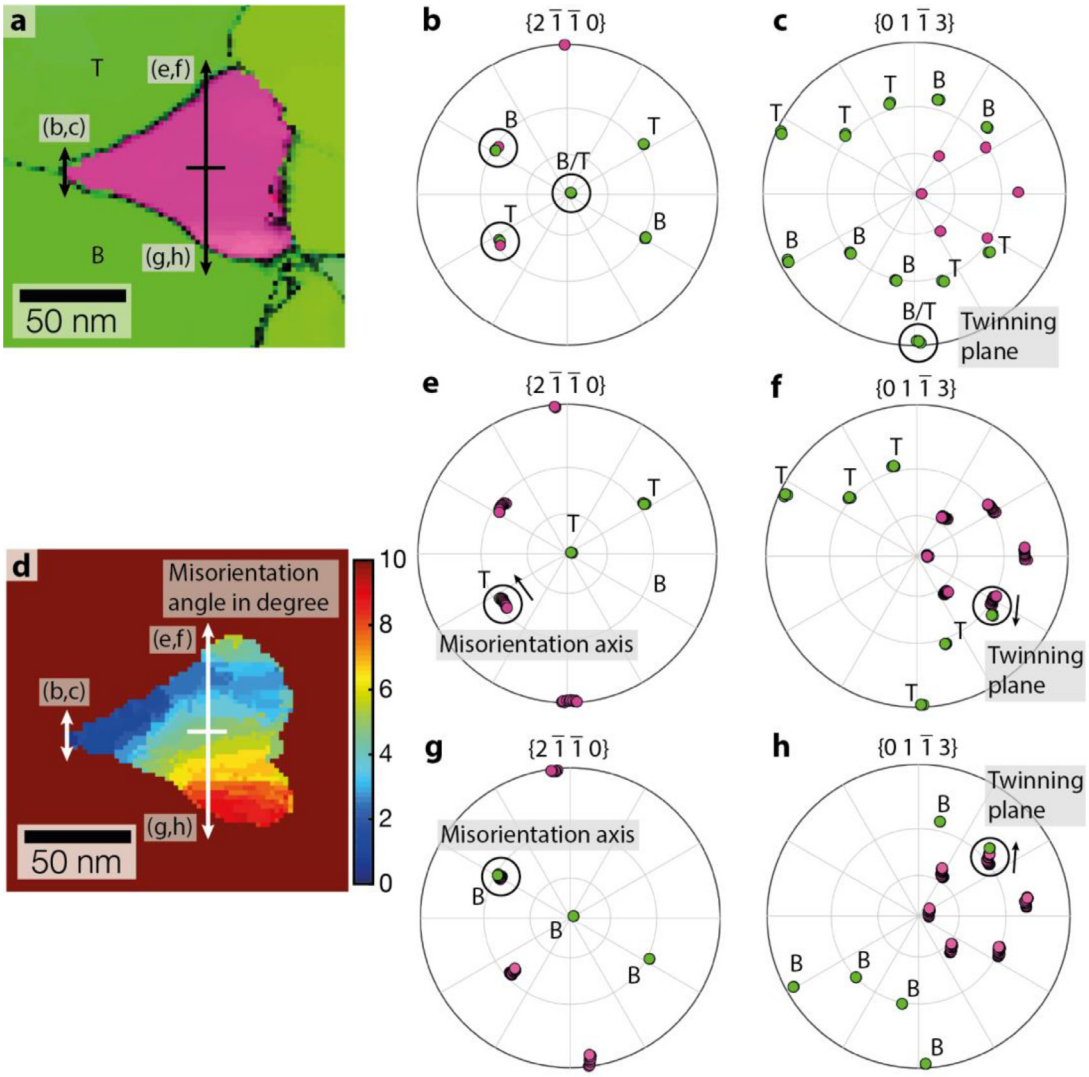

Fig. 4. Detailed analysis of the grain orientation relationships within a representative grain triplet. (a) Orientation map of the triplet around the triple junction, with the letters "T" and "B" designating the top and bottom twinned grains. The arrows indicate the lines along which the pole figures (b) and (c) and (e)–(h) have been plotted; the arrows for (e)–(h) start from the center of the grain. (b) and (c) show {2 1̄ 1̄ 0} and {0 1 1̄ 3} pole figures for the three grains, at locations very close to the triple junction. In (b) the black circles mark shared poles, while in (c) they correspond to the shared twin boundary between grains T and B. The orientation map in (d) is from the same region as in (a), but now colored by the misorientation angle that the local orientation forms with respect to the orientation at the triple junction. (e)–(h) present {2 1̄ 1̄ 0} and {0 1 1̄ 3} pole figures for orientations along the corresponding arrows in (a) and (d). The rotation of the pink-rose colored grain towards the two different twin orientation relationships is indicated by small arrows. The black circles mark the twinning planes and misorientation axes. (For interpretation of the references to color in this figure legend, the reader is referred to the web version of this article.)

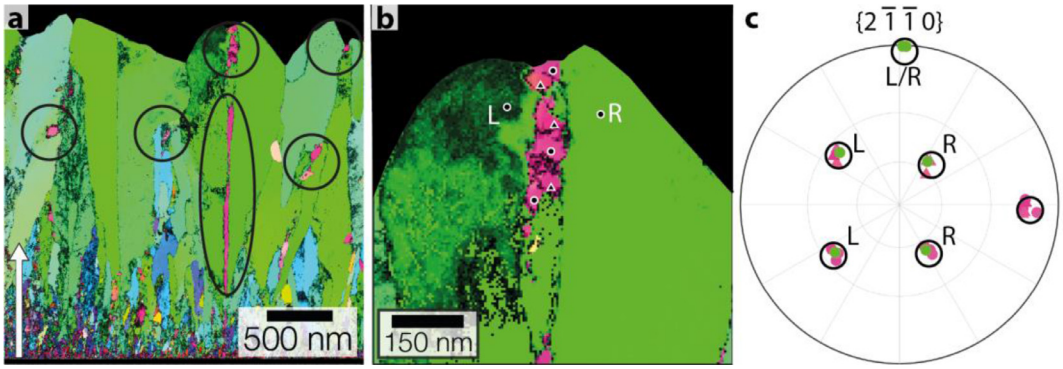

Fig. 5. Triple junction analysis in cross-section view. (a) Cross-section orientation map of the ZnO thin film, colored with respect to the film growth direction indicated by the arrow according to the color map in Fig. 2. A grain triplet, consisting of a large *a*-textured twin pair and a long, narrow (1 0 1̄ 3) oriented grain is indicated by the black ellipse. Above this, there is a zone of multiple, renucleating (1 0 1̄ 3) oriented grains. This is shown enlarged in (b), with the poles of selected grains shown in the {2 1̄ 1̄ 0} pole figure in (c). The two large (2 1̄ 1̄ 0) oriented grains are labeled in both (b) and (c) with "L" and "R" for left and right, respectively. The (1 0 1̄ 3) oriented grains are represented by triangles or disks in (b) and (c), depending on which orientation variant they belong to. Here, the black circles correspond to the {1 1 0} poles of an appropriately oriented zinc blende phase that could coordinate the green twinned grains and stimulate the growth of the (1 0 1̄ 3) oriented grains. (For interpretation of the references to color in this figure legend, the reader is referred to the web version of this article.)

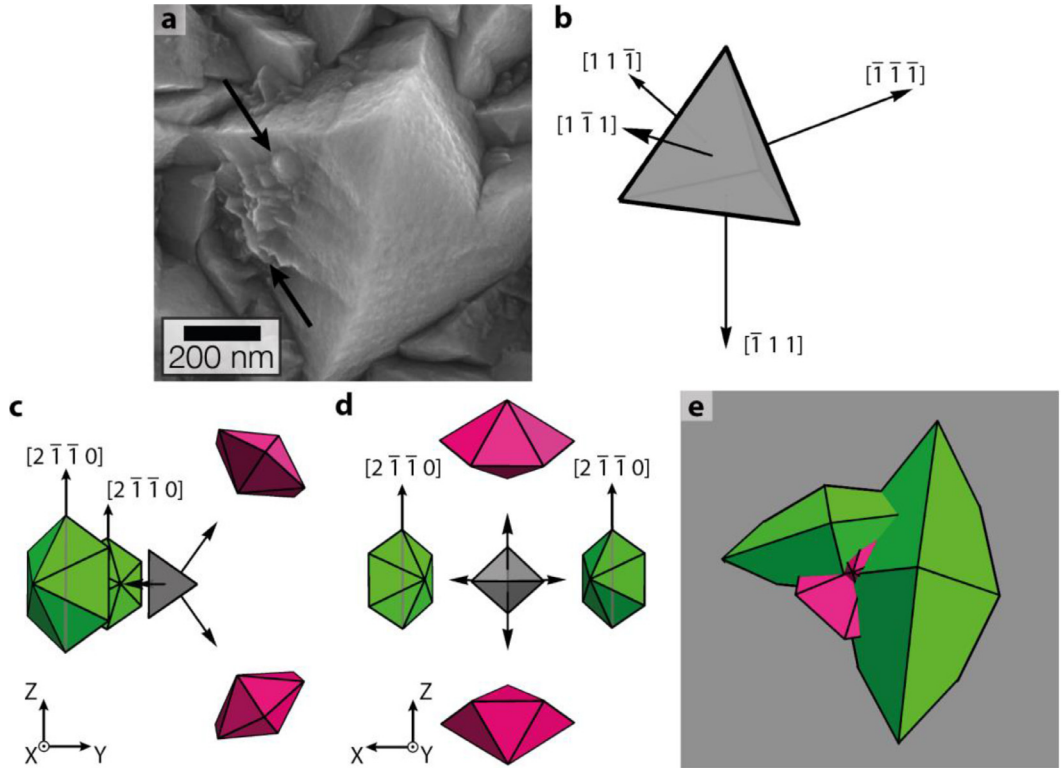

Fig. 6. Relation between the tetrahedral coordination of grains and the surface morphology. (a) SEM image showing re-nucleating grains between two large twinned grains that form a pyramidal surface structure. The re-nucleating grains appear either as narrow wedges or as small pointed caps. (b) represents the oxygen terminated {1 1 1} facets of a zinc blende tetrahedron. It is suitably rotated in (c) and (d) to coordinate four wurtzite grains according to the obtained results. The wurtzite grains are illustrated by hexagonal dipyramid forms that correspond to the idiomorphic grain growth shape for an *a*-textured film [16]. The two green grains have their [2 $\bar{1}$ $\bar{1}$ 0] fast growth axes parallel to the substrate normal, and so correspond to the *a*-texture twinned grains. Two facets of the zinc blende tetrahedron face these grains, leaving two other facets on which two other wurtzite grains can renucleate. These two other grains, in rose-pink, while "pointing" in different directions to each other, both conform to the (1 0 $\bar{1}$ 3) orientation relative to the substrate normal for renucleation. In (e) all four of these wurtzite grains are brought together, and adjusted in size, position and viewing angle in order to represent the SEM image in (a). (For interpretation of the references to color in this figure legend, the reader is referred to the web version of this article.)

and thereby explain subtle features in the surface morphology of the thin film. Fig. 6(a) shows a high magnification SEM image of an *a*-texture pyramid. In between the two grains forming the pyramid, small pointed caps and narrow wedges are visible; features of the type mentioned in the discussion of Fig. 1 at the beginning of Section 3. To explain how these features derive from the two orientations of renucleating grains, we consider the underlying polytypism mechanism, and the zinc blende core that tetrahedrally coordinates the four wurtzite grains. We expect that each wurtzite grain has their {0 0 0 1} plane parallel to an oxygen terminated {1 1 1} zinc blende plane [14], as illustrated in Fig. 6(b)–(d). The fast *a*-axis growth direction of the wurtzite grains is represented by the hexagonal dipyramid idiomorphic growth shape [16]. Two of them are the "successful" grains that form the twinned surface pyramid, having their *a*-axis parallel to the substrate normal, and so are colored in green. The other two correspond to the (1 0 $\bar{1}$ 3) textured grains, and so are colored in rose-pink. According to this geometry, each ⟨1 1 0⟩ edge of the zinc blende tetrahedron should be parallel to a ⟨2 $\bar{1}$ $\bar{1}$ 0⟩ direction shared between two wurtzite grains. In experimental accordance, black circles for the {1 1 0} poles of an appropriately oriented zinc blende phase are superimposed on the pole figure of Fig. 5(c), and agree well with the {2 $\bar{1}$ $\bar{1}$ 0} poles of the renucleating grains. In Fig. 6(e), these four grains have been scaled and brought together, while keeping their relative orientation relationship to each other, such that they represent the observation in Fig. 6(a). With the two green grains forming the surface pyramid, one of the renucleated rose-pink grains appears as a hexagonal cap, while the other appears as a sideways narrow angled wedge. This model therefore gives an excellent correlation to the features in the SEM images, permitting us to understand these small features that, in themselves, are inconsistent with growth by the van der Drift growth model [25].

While the phenomenological model that we present portrays well the influence of the ZnO triplets on the film microstructure and surface morphology, deeper questions remain concerning the underlying mechanistic causes. We know that the growth of ZnO grains in LP-MOCVD films is highly unstable to stacking errors, as observed from the abundance of stacking faults [15,17], which we have further implicated in the mechanism stimulating polytypism in *c*-texture films [14]. We have also hypothesized that enhanced growth at the concave surface of a twinned grain pair favors development of a pyramidal shape [16]. However, these concepts cannot fully account for the triplet growth nature, especially the development of the structural rotation that permits twinning on all three boundaries. Doing so may require an atomistic understanding of the flow, surface diffusion and incorporation of adatoms from the vapor phase, and better knowledge of the driving forces and energetics involved in forming the different structural components of the triplet.

4. Conclusions

We have presented a detailed analysis leading to a growth model of tetrahedrally-coordinated wurtzite-phase ZnO grain triplets within vapor-deposited *a*-texture polycrystalline thin films. The proof involves the correlation of TEM-based ACOM and high-resolution imaging of cross-section and plan-view samples with SEM surface imaging, and gives a self-consistent description of the

observed phenomena. Each grain triplet shares two features, which in themselves should be energetically unfavorable: a metastable zinc blende phase core; and an internal structural rotation of one of the grains that enables a coherent twin boundary configuration with both of its neighbors. Nevertheless, together all these aspects combine synergistically to give a stable/semi-stable form that is abundantly observed, such that the combined triplet structure must be energetically favorable under the film's growth conditions. Understanding better the underlying mechanisms behind the grain triplet formation presents a challenge for theoretical analysis and simulations. However, considering that the results correlate with observations of free-standing ZnO nanostructures, and that the tetrahedral coordination of grains and formation of coherent twin boundaries may be relevant for growth of wurtzite phase octet binary semiconductor compounds in general, these could be interesting questions to address in the future.

Declaration of Competing Interest

The authors declare that they have no known competing financial interests or personal relationships that could have appeared to influence the work reported in this paper.

Acknowledgements

The authors acknowledge funding from the SNSF, Grant Number 137833 (*ZONEM* project). We thank Prof. Christophe Ballif and Dr. Aïcha Hessler-Wyser of the Institute of Microengineering (IMT) Photovoltaics and Thin-Film Electronics Laboratory (PV-Lab) at EPFL, Dr. Lorenzo Fanni (formerly of the PV-Lab), and Dr. Sylvain Nicolay of the CSEM PV-Center at Neuchâtel for the provision of the ZnO thin film samples and for many useful discussions.

Supplementary materials

Supplementary material associated with this article can be found, in the online version, at doi:10.1016/j.actamat.2020.08.068.

References

[1] K.F. Kelton, A.L. Greer, Nucleation in condensed matter: applications in materials and biology, Pergamon, 2010.
[2] J.D. Verhoeven, Fundamentals of Physical Metallurgy, John Wiley & Sons, New York, 1975.
[3] D.A. Porter, K.E. Easterling, H.Y. Sherif, Phase Transformations in Metals and Alloys, third ed., CRC Press, 2008.
[4] V.G. Dubrovskii, Nucleation Theory and Growth of Nanostructures, Springer, Berlin, Heidelberg, 2014, doi:10.1007/978-3-642-39660-1.
[5] F. Glas, J.C. Harmand, G. Patriarche, Why does wurtzite form in nanowires of III-V zinc blende semiconductors? Phys. Rev. Lett. 99 (2007) 146101, doi:10.1103/PhysRevLett.99.146101.
[6] X. Yuan, P. Caroff, J. Wong-Leung, L. Fu, H.H. Tan, C. Jagadish, Tunable polarity in a III-V nanowire by droplet wetting and surface energy engineering, Adv. Mater. 27 (2015) 6096–6103, doi:10.1002/adma.201503540.
[7] S. Nicolay, S. Fay, C. Ballif, Growth model of MOCVD polycrystalline ZnO, Cryst. Growth Des. 9 (2009) 4957–4962, doi:10.1021/cg900732h.
[8] S. Faÿ, J. Steinhauser, S. Nicolay, C. Ballif, Polycrystalline ZnO: B grown by LPCVD as TCO for thin film silicon solar cells, Thin Solid Films 518 (2010) 2961–2966, doi:10.1016/j.tsf.2009.09.189.
[9] T. Koida, J. Nishinaga, H. Higuchi, A. Kurokawa, M. Iioka, Y. Kamikawa-Shimizu, A. Yamada, H. Shibata, S. Niki, Comparison of ZnO:B and ZnO:Al layers for Cu(In,Ga)Se2 submodules, Thin Solid Films 614 (2016) 79–83, doi:10.1016/j.tsf.2016.03.004.
[10] A. Favier, D. Muñoz, S. Martín de Nicolás, P.-J. Ribeyron, Boron-doped zinc oxide layers grown by metal-organic CVD for silicon heterojunction solar cells applications, Sol. Energy Mater. Sol. Cells. 95 (2011) 1057–1061, doi:10.1016/j.solmat.2010.11.013.
[11] M. Chen, Z.L. Pei, C. Sun, J. Gong, R.F. Huang, L.S. Wen, ZAO: an attractive potential substitute for ITO in flat display panels, Mater. Sci. Eng. B. 85 (2001) 212–217, doi:10.1016/S0921-5107(01)00584-0.
[12] C.-Y. Yeh, Z.W. Lu, S. Froyen, A. Zunger, Zinc-blende–wurtzite polytypism in semiconductors, Phys. Rev. B. 46 (1992) 10086–10097, doi:10.1103/PhysRevB.46.10086.
[13] H. Morkoç, U. Özgür, Zinc oxide: Fundamentals, Materials and Device Technology, Wiley-VCH, 2009.
[14] A.B. Aebersold, L. Fanni, A. Hessler-Wyser, S. Nicolay, C. Ballif, C. Hébert, D.T.L. Alexander, Zinc blende–wurtzite polytypism in nanocrystalline ZnO films, Acta Mater. 130 (2017) 240–248, doi:10.1016/j.actamat.2017.03.021.
[15] A.B. Aebersold, D.T.L. Alexander, C. Hébert, Height-resolved quantification of microstructure and texture in polycrystalline thin films using TEM orientation mapping, Ultramicroscopy 159 (2015) 112–123, doi:10.1016/j.ultramic.2015.08.005.
[16] A.B. Aebersold, L. Fanni, A. Hessler-Wyser, S. Nicolay, C. Ballif, C. Hébert, D.T.L. Alexander, Quantifying competitive grain overgrowth in polycrystalline ZnO thin films, Acta Mater. 173 (2019) 74–86, doi:10.1016/j.actamat.2019.04.049.
[17] F. Lorenzo, A.B. Aebersold, M. Morales-Masis, M. Ledinský, S. Escrig, A. Vetushka, D.T.L. Alexander, A. Hessler-Wyser, A. Fejfar, C. Hébert, S. Nicolay, C. Ballif, Direct imaging of dopant distribution in polycrystalline ZnO films, ACS Appl. Mater. Interfaces 9 (2017) 7241–7248, doi:10.1021/acsami.6b14350.
[18] E.F. Rauch, J. Portillo, S. Nicolopoulos, D. Bultreys, S. Rouvimov, P. Moeck, Automated nanocrystal orientation and phase mapping in the transmission electron microscope on the basis of precession electron diffraction, Zeitschrift Für Krist 225 (2010) 103–109, doi:10.1524/zkri.2010.1205.
[19] L. Dieterle, B. Butz, E. Müller, Optimized Ar+-ion milling procedure for TEM cross-section sample preparation, Ultramicroscopy 111 (2011) 1636–1644, doi:10.1016/j.ultramic.2011.08.014.
[20] E. Spiecker, Novel TEM methods for large-area analysis of misfit dislocation networks in semiconductor heterostructures, Philos. Mag. 86 (2006) 4941–4963, doi:10.1080/14786430600724447.
[21] A. Kobler, A. Kashiwar, H. Hahn, C. Kübel, Combination of in situ straining and ACOM TEM: a novel method for analysis of plastic deformation of nanocrystalline metals, Ultramicroscopy 128 (2013) 68–81, doi:10.1016/j.ultramic.2012.12.019.
[22] F. Bachmann, R. Hielscher, H. Schaeben, Grain detection from 2d and 3d EBSD data—Specification of the MTEX algorithm, Ultramicroscopy 111 (2011) 1720–1733, doi:10.1016/j.ultramic.2011.08.002.
[23] E.F. Rauch, L. Dupuy, Rapid spot diffraction patterns identification through template matching, Arch. Met. Mater. 50 (2005) 87–99 –00.
[24] A. Morawiec, E. Bouzy, H. Paul, J.J. Fundenberger, Orientation precision of TEM-based orientation mapping techniques, Ultramicroscopy 136 (2014) 107–118, doi:10.1016/j.ultramic.2013.08.008.
[25] A. van der Drift, Evolutionary selection, a principle governing growth orientation in vapour-deposited layers, Philips Res. Rep. 22 (1967) 267–288.
[26] Y. Ding, Z.L. Wang, T. Sun, J. Qiu, Zinc-blende ZnO and its role in nucleating wurtzite tetrapods and twinned nanowires, Appl. Phys. Lett. 90 (2007) 153510, doi:10.1063/1.2722671.
[27] Y. Ding, Z.L. Wang, Structure analysis of nanowires and nanobelts by transmission electron microscopy, J. Phys. Chem. B. 108 (2004) 12280–12291, doi:10.1021/jp048163n.
[28] A. Béré, A. Serra, Atomic structures of twin boundaries in GaN, Phys. Rev. B. 68 (2003) 033305, doi:10.1103/PhysRevB.68.033305.
[29] Y. Ding, Z.L. Wang, Structures of planar defects in ZnO nanobelts and nanowires, Micron 40 (2009) 335–342, doi:10.1016/j.micron.2008.10.008.
[30] A. Bastos, S. Zaefferer, D. Raabe, Three-dimensional EBSD study on the relationship between triple junctions and columnar grains in electrodeposited Co–Ni films, J. Microsc. 230 (2008) 487–498, doi:10.1111/j.1365-2818.2008.02008.x.